Giant Sea-Salt Aerosols and Warm Rain Formation in Marine Stratocumulus

JØRGEN B. JENSEN

National Center for Atmospheric Research, Boulder, Colorado

SUNHEE LEE

CSIRO Marine and Atmospheric Research, Aspendale, Victoria, Australia

(Manuscript received 7 September 2007, in final form 4 April 2008)

ABSTRACT

The concentrations and sizes of smaller aerosols (radius smaller than 0.5 μm) in the marine atmosphere vary owing to natural and anthropogenic factors. The concentrations and sizes of giant and ultragiant aerosols vary primarily due to wind-speed-dependent wave breaking. In climate models the formation of warm rain from marine stratocumulus clouds is usually parameterized based on the drops that form on the smaller aerosols. The present process study, using a stochastic Monte Carlo cloud model, shows that the variability of giant sea-salt aerosols and the variability of smaller aerosol cloud condensation nuclei are equally important in determining precipitation flux in marine stratocumulus. This strongly suggests that the effects of giant sea-salt aerosols should be included in the parameterization of warm rain formation in climate and other large-scale models.

The above results are based on highly detailed calculations of droplet growth in an idealized marine stratocumulus cloud; the authors believe that other marine stratus cloud conditions may change the calculated rain rates but that the conclusions regarding the relative importance of small and giant aerosols are robust.

1. Introduction

One of the main unknowns in the prediction of the future climate is the effect of anthropogenic aerosols on clouds and rainfall formation. Both anthropogenic and natural aerosols are thought to act as nuclei for cloud droplet formation. Increasing the aerosol concentration through anthropogenic emissions should theoretically increase the concentration of cloud droplets and simultaneously decrease their average size. For ice-free clouds (warm clouds) it has been hypothesized (Twomey 1977) that this would lead to more reflective clouds, thus countering the greenhouse warming and that it would also extend the cloud lifetime (Albrecht 1989) by reducing the cloud ability to form rainfall through coalescence of drops (warm rain processes).

Many climate and cloud models predict the onset of warm rainfall when the mean droplet radius exceeds a threshold value (Manton and Cotton 1977; Liu and Daum 2004; Rotstayn and Liu 2005). The parameterization of this so-called autoconversion process is based on properties of the majority of smaller drops, which are formed on smaller aerosol particles. However, if the drops that form the drizzle drops and raindrops are those that initially grew on the few larger aerosol particles, then a warm rain parameterization based exclusively on smaller drops would be in error. Other schemes also take into consideration spectral dispersion as well as liquid water (Berry and Reinhart 1973; Beheng 1994; Seifert and Beheng 2001; Liu and Daum 2004). Recently some mesoscale and large-scale models are including the effect of giant aerosols on warm rain formation (e.g., van den Heever et al. 2006; Posselt and Lohmann 2007).

The purpose of this study is to examine the relative importance of small and giant aerosol particles on precipitation formation. This is done by calculating droplet growth with a highly detailed stratocumulus model that traces the individual aerosol particles through many drop coalescence events and examines the aerosol sizes responsible for warm rain initiation. By varying the size

Corresponding author address: Jørgen Jensen, National Center for Atmospheric Research, P.O. Box 3000, Boulder, CO 80307-3000.
E-mail: jbj@ucar.edu

DOI: 10.1175/2008JAS2617.1

distribution of smaller aerosol particles, the effect of increased anthropogenic emissions on rainfall rate can be simulated, and by independently varying the wind speed over the ocean the effect of natural variability of larger sea-salt particles can be simulated. This allows for a calculation of the relative importance of the aerosol properties, which must be included in warm rain schemes for climate and other large-scale models.

This paper discriminates between smaller aerosol particles (dry radius, $r_d < 0.5$ μm), giant aerosol particles ($r_d > 0.5$ μm), and ultragiant aerosol particles ($r_d > 5$ μm). Variables used throughout the paper are defined also in Table 1. The giant aerosol particles are also commonly known as giant nuclei (GN) and the ultragiant aerosol particles as ultragiant nuclei (UGN). The discrimination between GN and UGN is arbitrary and, unless explicitly stated, the remainder of the paper will let giant aerosols refer to both GN and UGN.

The hypothesis that giant sea-salt particles could serve as the nuclei for raindrop formation was first proposed more than 50 years ago Woodcock (1950); it was subsequently discarded (Woodcock et al. 1971), but in more recent times it has again gained prominence (e.g., Johnson 1982; Feingold et al. 1999; Szumowski et al. 1999; Rosenfeld et al. 2002; Rudich et al. 2002). Giant aerosols, even insoluble particles, may potentially also contribute to warm rain formation over land (Johnson 1982) provided the particle sizes exceed 20–25 μm. In the present study the focus is on the marine boundary layer where the soluble aerosol particles are normally dominant.

Cloud dynamics may be very important for variability in rainfall from stratocumulus and other marine clouds (e.g., Stevens et al. 2005; Colón-Robles et al. 2006). The Colón-Robles et al. study demonstrated that updraft speeds near the base of marine trade wind cumulus clouds typically increase when the surface horizontal wind speed increases. However, the focus of the present study is a very sensitive evaluation of the microphysical processes under highly controlled (specified) dynamical conditions.

TABLE 1. Symbol list.

a, b	Parameters of CCN supersaturation spectra
e_s	Saturated vapor pressure
i	Index for small drop
j	Index for large drop
l_β	Condensation coefficient length
m_s	Salt mass
q_l	Cloud liquid water mixing ratio
r	Drop radius
r_c	Drop radius
r_d	Dry aerosol radius
r_e	Droplet effective radius
t	Time
z_b	Cloud base altitude
A	Autoconversion rate
C_0	Coalescence kernel sum
D_v	Vapor diffusivity
K	Thermal conductivity
L_v	Latent heat of vaporization
M_s	Molar weight of salt
M_w	Molar weight of water
N_a	Aerosol concentration, usually CCN
N_c	Total number of drops in the cloud volume
R	Rain rate
R_v	Gas constant for water
$\mathcal{S}$	Saturation ratio
S	Supersaturation in percent
T	Temperature
ν	Valence
ρ_s	Salt density
ρ_w	Liquid water density
σ	Surface tension of liquid water against air
σ_r	Droplet spectral width
τ	Actual time until next coalescence event
τ'	Median time until next coalescence event
Φ	Practical osmotic coefficient
χ_s	Giant sea-salt spectrum

2. Aerosol spectral variability

Figure 1 shows cumulative aerosol spectra as observed in marine air. The dashed curve shows measurement from summertime marine background air from Cape Grim in Tasmania (Gras 1995). These naturally occurring aerosol particles smaller than about 1-μm dry radius consist mainly of sulfates, some sea salt (Ayers and Gras 1991), and possibly organic material. In many other regions, the submicrometer aerosol particles may occur in much higher concentrations and they may be dominated by anthropogenic sources. Heavily polluted air could possibly contain 100 times more than the 400 cm^{-3} summer average observed at Cape Grim.

Figure 1 also shows measurement of giant aerosol particles, consisting of sea salt, from marine air near Hawaii and Bermuda (Woodcock 1953). The giant aerosol data are stratified by wind force, which is here expressed as wind speed (Simpson 1906). These measurements are chosen because they represent a direct measurement of the salt particle size, as opposed to more recent optical probe measurements that measure a solution drop size with an unknown amount of salt inside. The giant sea-salt size distributions show a huge natural variability. For instance, the concentration of aerosol particles with $r_d > 5$ μm vary by six orders of magnitude for winds in the range 1–35 m s^{-1}; in relative terms, this wind-speed-induced variation is typically larger than the natural and anthropogenic variability of smaller accumulation-mode aerosol particles with radii of about 0.1 μm. Figure 1 also shows that the maximum

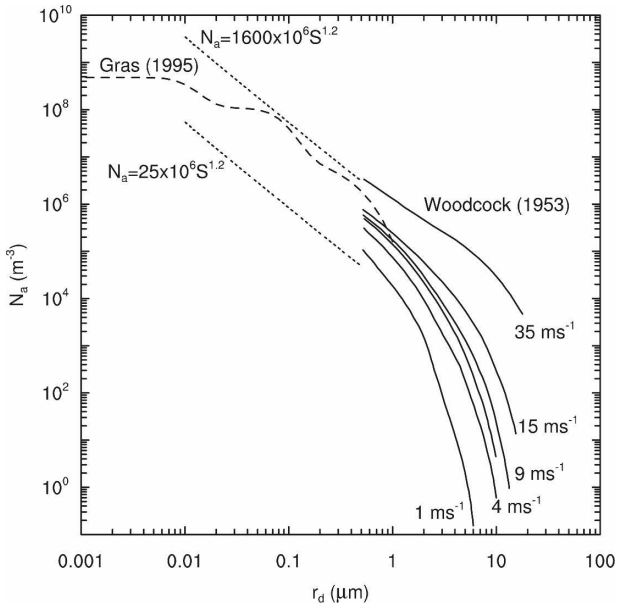

FIG. 1. Cumulative aerosol concentration N_a as a function of dry aerosol radius r_d. The dashed curve shows modal fits to long-term measurements of aerosol particles at Cape Grim, Tasmania (Gras 1995). The two dotted curves show aerosol size distributions calculated from supersaturation spectra by assuming a composition of ammonium sulfate particles; for brevity these aerosol size distributions are labeled with the corresponding supersaturation spectral values. The solid curves show wind speed dependent size distributions (Woodcock 1953) assuming a composition of sodium chloride and with the wind-force curves labeled with the corresponding wind speed (see text).

size of giant sea-salt aerosol particles increases with wind speed. Other measurements in Woodcock (1953) show that the total aerosol mass at a given wind force may be a factor of 2–3 higher or lower than the mean mass. There have been many other measurements of sea-salt size distributions as a function of wind speed [e.g., O'Dowd et al. (1997); see also a review in Lewis and Schwartz (2005)]. These were mostly for measurements close to the sea surface, whereas Woodcock's (1953) measurements, shown in Fig. 1, were obtained near cloud base. For a given wind speed, the scatter in the many surface measurements is often significant; some of this may be due to sampling method as well as differences in sea state, fetch, stationarity of the wind, etc.

Aerosol particles in the marine boundary layer are generally soluble and act as nuclei for cloud droplet formation. The cumulative concentration N_a of cloud condensation nuclei (CCN), which activate into cloud droplets, is a function of water vapor supersaturation S (%). Supersaturation spectra frequently show considerable variation but are often simplified as $N_a = aS^b$, where a and b are fitted constants (see, e.g., Hegg and Hobbs 1992). The dotted lines in Fig. 1 denote two supersaturation spectra corresponding to very clean marine air ($N_a = 25 \times 10^6\ S^{1.2}\ \mathrm{m}^{-3}$) and polluted air ($N_a = 1600 \times 10^6\ S^{1.2}\ \mathrm{m}^{-3}$). The supersaturation spectra expressed as power laws do not capture the typical modal structure of smaller aerosol particles, but the power laws are nevertheless commonly used to characterize CCN spectra.

Measurements of marine aerosol have demonstrated that increasing wind speed leads to an increase in the concentrations of both small and giant aerosols; for instance, Smith et al. (1989) examined the concentrations of particles with ambient radii in the range of 0.09 to 0.25 μm. Their results show that increasing the wind speed from 4 to 8 m s^{-1} and from 8 to 16 m s^{-1} increased the particle concentrations by about 30% and 70%, respectively. In another study, Bigg et al. (1995) examined the concentration of CCN active at 0.6% supersaturation; their results showed that the above wind speed changes led to CCN increases of 50% and 100%, respectively. Other measurements by O'Dowd and Smith (1993) shows that the combination of sea salt and other types of aerosols in the size range of 0.05–1.5-micron radius are not well correlated with wind speed in the marine boundary layer. For giant aerosols with radius larger than 5 μm, the increases in concentrations are typically an order of magnitude larger for the same increases in wind speed (from 4 to 8 m s^{-1} and from 8 to 16 m s^{-1}). The strongest relative increase in particle concentration with wind speed is thus associated with the giant aerosol particles.

Marine stratocumulus, CCN, and cloud droplet concentrations

The purpose of the present paper is to determine if the range of rainfall rates in warm, marine stratocumulus is more dependent on the variability of small or of giant aerosol particles.

The range of small aerosol particles, specifically CCN, has been measured in a number of studies over the ocean (e.g., Yum and Hudson 2004, Hudson and Xie 1999). For measurements taken during the Southern Ocean Cloud Experiment (SOCEX-1) (Boers et al. 1996), Yum and Hudson (2004) found average wintertime CCN concentrations at 1% supersaturation of about 30 cm^{-3} close to sea surface. For summertime nights (SOCEX-2) (Boers et al. 1998) in the same area west of Tasmania, Yum and Hudson found average CCN values of 200–300 cm^{-3}. High CCN concentrations (at 1% supersaturation) were found by (Hudson and Xie 1999) in the Northern Hemisphere eastern oceans (126–1063 cm^{-3}).

For the present modeling study, it may be more relevant to ensure that the observed range of cloud droplet concentrations matches that used for our model study. Examples of direct measurements of cloud droplet concentrations in marine stratocumulus using aircraft probes give ranges of 10–200 cm^{-3} in Southern Ocean clean marine background conditions (Boers et al. 1996,[1] 1998; Boers and Krummel 1998); 18–370 cm^{-3} near the coast of Nova Scotia and in the Canadian Arctic (Peng et al. 2002, concentrations read off their Fig. 2); 55–244 cm^{-3} near Tenerife in the Atlantic Ocean (Pawlowska and Brenguier 2000); 59–207 cm^{-3} (Stevens et al. 2003a) off California, and 43–289 cm^{-3} also off California (Lu et al. 2007). Thus, for the present study we will select a CCN spectrum range such that a cloud droplet concentration range of about 20–400 cm^{-3} is simulated. It is, however, also possible that higher cloud droplet concentrations may occur in highly polluted continental outflow air. The approximate range of 20–400 cloud droplets cm^{-3} is wider than the satellite estimates of Bennartz (2007), who found mean concentrations of 40–67 cm^{-3} for the Southern Hemisphere and 64–89 cm^{-3} for the Northern Hemisphere.

Giant sea-salt particles range, as detailed above, considerably as a function of wind speed, but 16 m s^{-1} is a reasonable upper wind speed for marine stratocumulus. The highest wind speeds for which we have observed marine stratocumulus is 16 m s^{-1} at an altitude of 35 m (Australian King Air as part of the ACE-Asia/APEX-E2 deployment). As with the small aerosol particles, it is possible that values exceeding 16 m s^{-1} may occur. The majority of aircraft experiments in marine stratocumulus have focused on regions with a high frequency of occurrence of suitable clouds. This may have skewed the sampling so as to not include regions with rare occurrences of more extreme wind speeds during marine stratocumulus situations.

3. Model description

The present calculations employ an adiabatic parcel model with condensation and stochastic coalescence. The adiabatic assumption implies that the parcel does not mix with the surrounding air, that radiative heat exchanges can be ignored, and that sedimenting droplets are assumed to remain in the parcel. Coalescence is implemented using a Monte Carlo method (Gillespie 1975, hereafter G75) to calculate gravitational coalescence; this makes the model extremely computationally intensive.

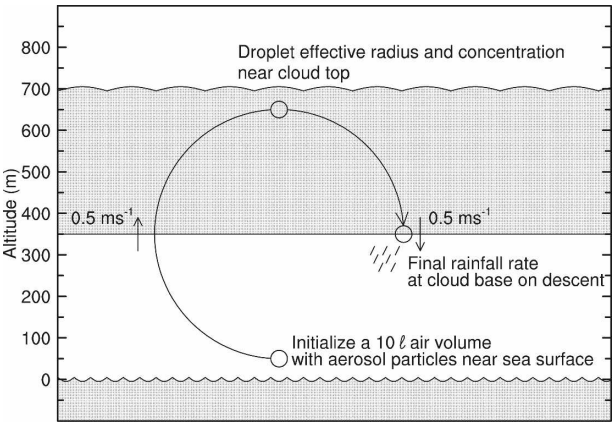

FIG. 2. Stratocumulus cloud and some modeling conditions. Parcels are initialized at 50-m altitude with no updraft and rise to 650 m where the updraft once again becomes zero before accelerating down to cloud base. The updraft profile follows a cosine function of time, the period being 3770 s. Thus, the parcel is cloudy for 1885 s, and the maximum updraft and downdraft of 0.5 m s^{-1} is at cloud base.

The model will be used for simulating a single marine stratocumulus. A simple kinematic calculation is employed to move an air parcel in a cyclical motion from near sea surface, upward through cloud base to cloud top, and then again down to the cloud base; see Fig. 2. The highest updrafts and downdrafts of 0.5 m s^{-1} occur at cloud base. A complete aerosol spectrum is specified near the sea surface, and the resulting drop spectrum and rainfall rate is evaluated once the parcel has ascended to cloud top and descended to cloud base; thus, rainfall rate is evaluated as the parcel descends through the cloud base. Both condensation and coalescence is calculated throughout the ¾ circular motion. We assume that all aerosols and droplets remain in the parcel; that is, sedimentation of droplets out of the parcel is not accounted for. This is obviously a simplification and it can be argued that this will lead to the model overestimating rainfall rates, but the implications are not straightforward. For instance, G. Vali (2007, personal communication) has observed drizzle being suspended and growing in updrafts in marine stratocumulus, with the result that drizzle drops eventually may fall out of the updrafts in marine stratocumulus. Such a scenario is not accounted for in the present model. A number of other effects are likewise omitted in the present calculations; the effect of radiative cooling of cloud droplets (Barkstrom 1978) is omitted because it is only important for the relatively small amount of time the drops are present in the uppermost tens of meters in the cloud, and recirculation of air is omitted—not because

[1] Reanalysis, using a more stringent requirement to avoid drop-free holes within a 1-s sample, shows that 20 cm^{-3} is a more realistic lower limit for the average drop concentration.

it does not occur, but because we wish to determine the most significant aerosol effect on warm cloud precipitation formation based on a single cycle through the cloud.

The thermodynamic conditions and updraft speed utilized in the model runs are loosely matched to observations from the NSF/NCAR C-130Q research aircraft as obtained during the Second Dynamics and Chemistry of Marine Stratocumulus (DYCOMS-II) experiment off the coast of California (Stevens et al. 2003a,b). Our calculated maximum liquid water mixing ratio of 0.58 g kg^{-1} (50 m below cloud top) compares well with that of Stevens et al. (2003a), which has an average maximum liquid water content of 0.69 g kg^{-1} based on nine flights. It is important to note that all of our runs have the same maximum liquid water mixing ratio and the same time spent in cloud; thus the only differences in calculated rainfall rate are solely due to variations in aerosol size distributions.

The model is used to simulate a typical well-mixed cloud of moderate thickness, thus making the study representative for many natural marine stratocumulus.

a. Aerosol specification, parcel air volume, and number of size classes

A series of model runs are conducted in which the size spectra of smaller aerosol particles ($r_d < 0.5$ μm) and giant aerosol particles ($r_d > 0.5$ μm) are varied independently to evaluate the relative impact of anthropogenic changes (assumed confined to smaller aerosol particles) and wind speed changes (assumed confined to giant aerosol particles). This is done by prescribing the small aerosol particles as supersaturation spectra of the form $N_a = aS^{1.2}$. The value of a is varied over the range from 25 to 1600 ($\times 10^6$ m^{-3}), and these smaller aerosol particles are assumed to consist of ammonium sulfate. Giant aerosol particles are approximated as sodium chloride particles for which the size distribution is specified using interpolation between wind-force-dependent size distributions (Woodcock 1953) over the wind speed range 1–16 m s^{-1}.

Note that we do not use "size bins" and "bin width" of aerosols and droplets in the normal sense; rather, in the present study we define a "size class" for which all the particles have the identical sizes. The ammonium sulfate aerosols are specified using 450 size classes covering $r_d < 0.5$ μm, and the sodium chloride distribution using 35 size classes covering $0.5 < r_d < 17.5$ μm. All model runs use a parcel volume of 10 L air. A 10 L volume yields good results for the Monte Carlo simulation; however, very rare interactions that occur among drops in larger volumes cannot be included. The

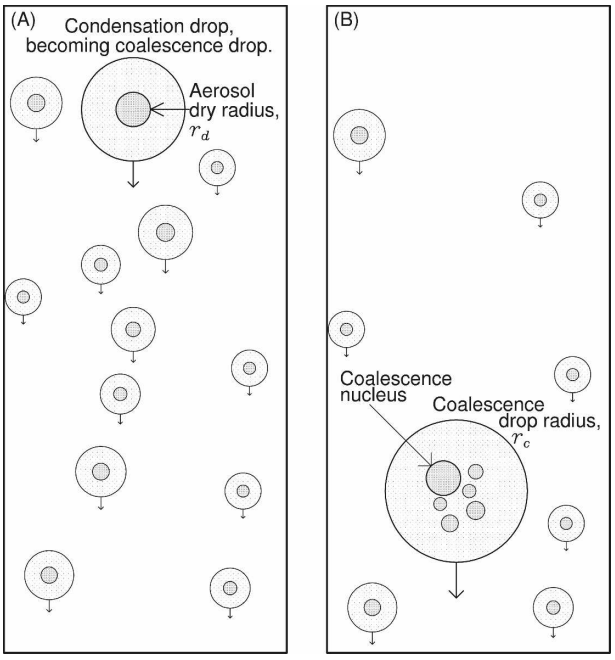

FIG. 3. Coalescence drop development and the principle of a coalescence nucleus. (a) A number of condensation drops with their respective dry aerosol particles (CCN) shown schematically inside. (b) The largest condensation drop initiates coalescence and eventually captures five smaller drops. Only one CCN nucleus is a coalescence nucleus for each coalescence drop; this particular nucleus is labeled r_d in (a) and "coalescence nucleus" in (b).

Monte Carlo implementation ensures that, once a coalescence event takes place, the two coalescing drops are removed from their size classes, and a completely new size class is created. The single drop in the new size class is then subject to condensation and further coalescence like the drops in all the other size classes. The creation of a new size class after each coalescence event results in the total number of size classes increasing with time, which is computationally intensive, but it ensures negligible numerical broadening of the drop spectrum.

Aerosols are traced through coalescence events and this results in particularly high computational demands; accordingly, only a few runs were done with aerosol tracing. The principle of aerosol tracing is demonstrated in Fig. 3. The left box shows a number of condensation drops with their nucleus size shown schematically inside; large condensation drops form on large CCN and small condensation drops on small CCN, as is expected for the present calculation using fully soluble aerosol particles. If a drop grown purely by condensation becomes so large that it by chance collects a smaller drop below it, then the initial nucleus in the large drop will be termed a "coalescence nucleus." The

newly formed coalescence drop thus contains the aerosol mass from its two "parent drops." The present stochastic coalescence model is implemented in such a way that tracing is done for all aerosols within a drop; that is, at the end of the calculation the single coalescence nucleus within each coalescence drop is determined. This allows one to determine which part of the aerosol spectrum is responsible for the formation of the significant precipitation drops, thus answering the question: Are precipitation drops mainly initiated by initial coalescence between condensation drops formed on the numerous small aerosol particles (e.g., accumulation mode aerosol particles) or is it necessary to have giant or ultragiant aerosol particles to initiate the formation of drizzle drops?

Drop growth is calculated for a parcel volume initially of 10 L; this volume changes by a small amount owing to the change of density as parcels move up and down. The number of coalescence events in a 10-L cloud volume leads to a very computer intensive calculation, primarily because the collection kernel sums change due to condensation and thus need to be recalculated after each coalescence event.

For the stochastic coalescence model (G75), the model particle spectrum initially contains about 485 size classes; each coalescence event creates a new size class with one drop in it. Both the original and the new size classes are followed independently in terms of drop radius, solute mass, and precursor drops. In a 47-min model run, which takes the air parcel from near the surface to the cloud top and back to cloud base, the number of size classes increases from 485 to values in the range from 5000 to 340 000, and this results in a very lengthy calculation for each air parcel. It would be desirable to use a parcel volume larger than 10 L, but increasing the modeled cloud volume from 10 L to 1 m^3 would increase the CPU time a million times.

b. Initialization of drop sizes

Solution drop sizes were initialized based on the ambient saturation ratio (0.8553) at 50-m altitude above sea level. The solution drop sizes at 50-m altitude (300 m below cloud base) were calculated assuming that they are in equilibrium with the ambient humidity.

For initializing, we use the Pruppacher and Klett's (1978, hereafter PK78) Eq. (6.26b) to calculate the size of solution drops in equilibrium with the ambient humidity. Based on the salt particle size and composition, we calculate the droplet molality [PK78 Eq. (4.63b)]. Based on the molality, the practical osmotic coefficient Φ [see PK78 Eq. (4.68)] was determined by linearizing the tabled values of Φ for sodium chloride (Low 1969) and ammonium sulfate (Robinson and Stokes 1959).

For initializing solution drop sizes, we solve the PK78 Eq. (6.26b) by iteration to determine a consistent pair of values for r and m_s that matches the ambient saturation ratio to $\mathcal{S} = 0.8553$. This saturation ratio applies to an altitude of 300 m below cloud base.

c. Condensation model

The simplest model calculation of drop growth is the adiabatic Lagrangian parcel model. Adiabatic parcel model equations have been presented in a number of studies beginning with Howell (1949), and we use a slightly modified version of the equations given in Jensen and Charlson (1984).

In the present study the development of large aerosols from some distance below cloud base will be followed up toward the inversion. The exponential term in the droplet growth equation is retained as droplet condensation is initiated at the 300-m cloud base where the solution drops are highly concentrated. The expression for the condensation coefficient (Fukuta and Walter 1970) is included to account for accommodation effects: The droplet growth equation, applied to the ith drop, is therefore

$$\frac{dr_i}{dt} = \frac{1}{r_i}\frac{\mathcal{S} - \exp\left\{\dfrac{2\sigma}{R_v T \rho_w r_i} - \dfrac{\nu\Phi m_{si} M_w}{M_s[(4\pi/3)\rho_w r_i^3 - (m_{si}\rho_w)/\rho_s]}\right\}}{\dfrac{L_v^2 \rho_w}{K R_v T^2} + \dfrac{R_v T \rho_w (r_i + l_\beta)}{D_v e_s r_i}}. \quad (1)$$

Here the practical osmotic coefficients Φ of sodium chloride are taken from Low (1969) and those of ammonium sulfate from Robinson and Stokes (1959). A condensation coefficient of 0.04 is used in the calculation of l_β (see Fukuta and Walter 1970). Coalescence events may bring ammonium sulfate aerosols and sodium chloride aerosols together in the same drop. In that case, the solute term is calculated used the appropriate summation of the two chemical components (in particular, terms ν, Φ, m_{si}, M_s, and ρ_s).

Four differential equations for the change in water vapor mixing ratio, temperature, air density, and altitude are the same as in Jensen and Charlson (1984), and pressure is diagnosed from the equation of state including virtual temperature effects of water vapor. In this study the updraft speed w will be specified using a cosine function to give a circular motion (see Fig. 2).

Note that the droplet growth equation is applied to each drop size class in the cloud volume used in this study.

d. Stochastic Monte Carlo model

The stochastic coalescence model (G75) is used to calculate the gravitational coalescence among drops in a fixed volume of cloudy air. The advantage of this model is that there is no numerical diffusion as a result of a coalescence event. For the cloudy volume, the G75 model calculates the probability of any drop being captured by and coalescing with any larger drop. The Gillespie model is implemented using the "fully conditioned" method (see G75).

By ranking the coalescence probabilities, the G75 model can be used to calculate the time τ until the next coalescence event, the size class of the small drop, i, that is captured, and the size class of the large drop, j, that captures drop i. By drawing three random numbers for each coalescence event, the drops involved and the time until the next coalescence event can be calculated. During the time between coalescence events, the condensation model is used to calculate drop size changes.

e. Collision, coalescence, and collection efficiencies

A number of studies have determined the collision efficiency using numerical calculations (e.g., Hocking 1959; Davis and Sartor 1967; Hocking and Jonas 1970; Klett and Davis 1973; Schlamp et al. 1976; Davis 1984). In contrast, there have been relatively few studies that have attempted to determine collection efficiencies by experimental means (e.g., Woods and Mason 1964; Beard and Ochs 1983). Most experiments have studied collection efficiency for relatively large drops. In the present study, the collision efficiencies for collector drops larger than 10-μm radius are taken from Klett and Davis (1973). The collision efficiencies of smaller droplets have been examined by Rogers and Davis (1990), which included van der Waals forces between droplets. The Rogers and Davis study shows collision efficiencies that are larger for very small collector droplets than they are for, say, 10-μm droplets. Collision efficiencies from Klett and Davis (1973) and Rogers and Davis (1990) are used for collector drops up to 60-μm radius; larger drops are assumed to have the same collision efficiencies as 60-μm drops. The collision efficiencies were also not allowed to exceed unity since no observational data have shown larger values.

Once drops collide, it is assumed that drop coalescence will take place; that is, the coalescence efficiency is unity. The product of the collision and coalescence efficiencies is the collection efficiency. Droplets of $r <$ 2 μm are assumed not to be collected.

f. Drop terminal velocity

The terminal velocity for a given drop radius depends on air pressure and temperature. Drop terminal velocity is calculated for drop radii in a number of hydrodynamic regimes (Beard 1976). For efficiency of computation, we tabled the terminal velocity in increments of 1-μm drop radius up to 1000 μm. Before calculating the collection kernels, the tabled terminal velocity values were interpolated as a function of drop radius so that drops of near similar sizes would not have zero terminal velocity difference.

Two tables of terminal velocity were created corresponding to two altitudes in the cloudy boundary layer; a second interpolation of terminal velocity was then done, this time as a function of parcel altitude.

g. Integration time steps

Below cloud base the calculation of condensational growth of solution droplets can become unstable unless very small time steps are used. This is because the small aerosol spectrum contains particles as small as 14-nm dry radius; for the calculations corresponding to the cleanest conditions (few small aerosol particles) this is necessary to ensure that the parcel contains both activated and unactivated droplets above the altitude of the main supersaturation peak (a few tens of meters above cloud base). If the calculations did not include such small aerosol particles, then the calculated drop concentrations and thus the mean cloud droplet radii would be in error in some of the cases. The penalty for including very small aerosol particles comes through the requirement for very short time steps, but condensational growth requires only a small fraction of the total computer time. A time step of 0.0002 s or shorter is used below cloud base; otherwise a time step of 0.002 s is used in the condensation calculation using a fourth-order Runge–Kutta scheme. Above cloud base the model continues to calculate condensational growth of both activated and unactivated aerosol particles.

After coalescence has commenced, the condensation time step is adjusted depending on the time between coalescence events in such a way that it never exceeds 0.002 s. If the calculated time between coalescence events is less than 0.002 s, then the condensation time step is set to the time between coalescence events.

h. Condensational change to collection kernels

Near cloud base all droplets are very small; this results in the value of the collection kernel sum C_0 [see G75 Eq. (18)] being so small that the time until the next coalescence event τ [G75 Eq. (19a)] may become very large. For a cloud volume of 10 L, τ may thus exceed

the lifetime of the cloud. Yet, near cloud base the condensational growth of droplets is very fast, and this means that collection kernel sum rapidly increases as the air moves upward from the cloud base; hence τ rapidly becomes smaller. We have chosen to reconcile this problem in the following manner: The estimated median time, τ', until the next coalescence event, is calculated from [see also G75 Eq. (19a)]

$$\tau' = C_0^{-1} \ln(1/0.5). \quad (2)$$

Here C_0 is the coalescence kernel sum [see G75 Eq. (18)]. If this median time is greater than 1 s, the condensational growth is calculated for 1 s, after which τ' is reevaluated. If τ' is less than 1 s, then the actual value of τ from G75 Eq. (19a) is used for the time to the next coalescence event and for the duration of condensational growth. This procedure is, in practice, only invoked in the first few tenths of meters above cloud base since the collection kernel sum increases rapidly above cloud base. The calculation of rain-rate development is nearly insensitive to the choice of the 1 s; any value shorter than about 100 s would give almost the same number of coalescence events during the parcel's time in cloud.

i. Thermodynamic conditions

The parcel was initiated 50 m above sea level with a pressure of 1008.75 hPa, a temperature of 289 K, and a saturation ratio of 0.8553. This yields a cloud base (relative humidity of 100%) altitude of about 350 m with very small variations caused by the amount of condensed water on aerosol particles; this varies with the specification of aerosol particles size distributions.

4. Results: The nuclei of raindrop formation

Figure 4 shows an example of the results of aerosol tracing to determine the coalescence nuclei for a 10-L cloud volume with giant aerosol particles corresponding to an 8 m s^{-1} wind speed and a CCN spectrum of 200 $S^{1.2} \times 10^6$ m^{-3} for the smaller aerosol particles. The abscissa shows the dry aerosol radius r_d at the onset of the calculation. The ordinate shows the final drop radius r_c on descent to the cloud base. The solid line shows the results in the absence of coalescence, that is, the condensational relationship between drop and aerosol size as the drop passes through cloud base on descent. Importantly, cloud base is here defined to be the altitude where the parcel initially became supersaturated on ascent. Figure 4 also shows the coalescence nucleus size and the corresponding drop size for all coalescence drops; each of the 8219 circles corresponds to a single coalescence drop. About 932 000 aerosol particles activated cloud droplets; thus only a small fraction of these participated in coalescence events. Those that did not participate in coalescence events have sizes that fall essentially on top of the "condensation only" curve.

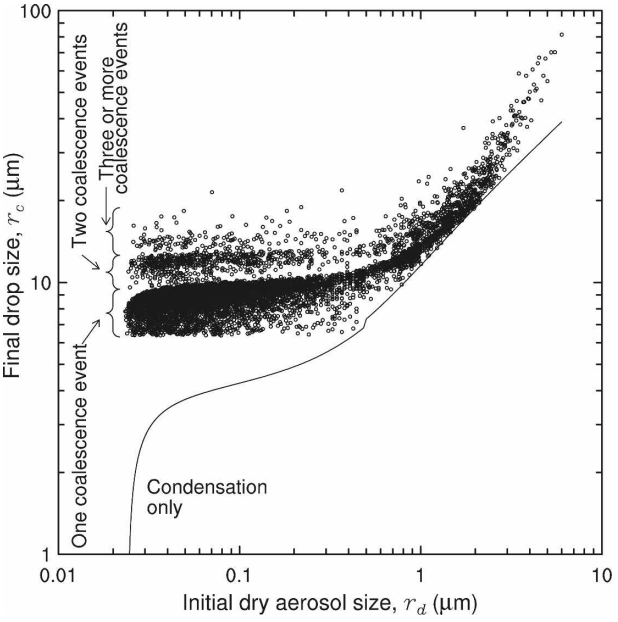

FIG. 4. Final drop size r_c on descent through cloud base as a function of initial dry aerosol size r_d. The solid curve shows the relationship for condensation only (no coalescence allowed); the slight discontinuity of the curve at $r_d = 0.5$ μm is caused by the assumption of small aerosols consisting of ammonium sulfate and larger aerosol particles consisting of sodium chloride. Each of the 8219 circles show the relationship between coalescence nuclei size and final drop size. Among coalescence drops formed on smaller aerosol particles it is possible to see three somewhat separate families of points: those that have undergone one, two, and three or more coalescence events.

The tracing of aerosol particles for the above example demonstrates that the vast majority of coalescence drops are initiated by drops initially formed on small aerosol particles, which capture even smaller drops. More than 90% of the coalescence nuclei are smaller than 0.5 μm radius, with giant nuclei accounting for only 9.5% of the coalescence drops. For comparison, the concentration of giant aerosol particles is less than 0.5% of the total concentration of activated drops, thus demonstrating that the giant aerosols in this case are 20 times more efficient at forming coalescence drops.

Figure 4 also shows several "families" of coalescence drops formed on small aerosol particles. One group consists of coalescence drops formed by a single coalescence event; these coalescence drops have maximum

sizes of about 10-μm radius on descent at cloud base. This group of drops is skewed toward the 10-μm radius because most coalescence events between smaller drops take place near cloud top where these drops are largest. The few coalescence drops positioned immediately above the solid line correspond to coalescence events taking place closer to cloud base on either ascent or descent. The second family of particles in Fig. 4 has radii in the range 10–13 μm; these are mostly from drops formed by two coalescence events. A third family of drops has radii at or above 15 μm; these consists mainly of drops that have undergone three or more coalescence events.

Only a few drops formed on coalescence nuclei smaller than 0.5 μm dry radius grew to sizes of 20 μm or larger at cloud base on descent. In contrast, many coalescence drops that formed on giant, and in particular on ultragiant, aerosol particles grew readily to much larger sizes. Thus, even if some drops in the main cloud droplet peak (those that form on small aerosol particles) manage to become coalescence drops, their small size will not allow them to compete efficiently in the race to form drizzle drops; the drops formed on giant and ultragiant aerosol particles grow rapidly by both condensation and coalescence, and they therefore win the race to form precipitation drops.

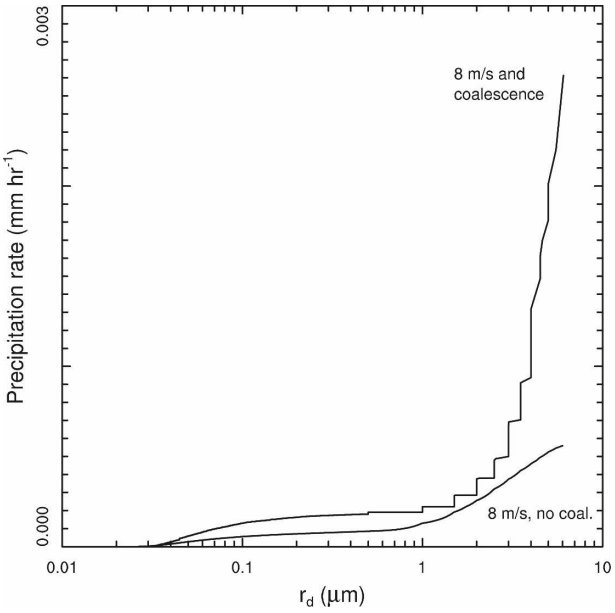

FIG. 5. Cumulative rain rate for drops initially formed on aerosols smaller than dry radius r_d. The example is for a CCN spectrum given by $N_a = 200 \times 10^6\ S^{1.2}$ m^{-3} and giant nuclei corresponding to a Woodcock distribution at 8 m s^{-1} wind speed. The two curves correspond to a calculation with stochastic coalescence and one with no coalescence.

5. Results: Rainfall rate as a function of small and giant aerosol particles

Figure 5 shows the cumulative rainfall amount at cloud base as a function of the dry particle radius r_d. Two curves are shown, each of which has the same aerosol size distribution for both small and giant aerosols; one curve shows the result for a calculation with condensation only (labeled "no coalescence") and another calculation shows the result for a calculation with both condensation and coalescence included. For the latter calculation, Fig. 5 shows that roughly half the precipitation flux originates on coalescence nuclei with $r_d > 4$ μm; thus, the impact of the few largest giant aerosols is very important.

Figure 6 shows the calculated rainfall rate R at cloud base on descent plotted as a function of droplet effective radius r_e (Hansen and Travis 1974) at cloud top. The reason for using r_e rather than the mean cloud droplet radius $\bar{r}_c$ is that satellite studies (e.g., Rosenfeld and Lensky 1998) have attempted to relate the state of precipitation development to the effective radius at cloud top.

The solid curves in Fig. 6 pertain to results using a given giant aerosol size distribution (wind speed dependent distributions, labeled in m s^{-1}); high wind speed conditions are in the top part of the figure. The dashed curves pertain to results using a given size distribution of small aerosols (supersaturation spectra, labeled aS^b); clean air results (few small aerosol particles) are shown in the right part of the figure, and more polluted cases are in the left part of the figure. The figure also shows the approximate cloud droplet concentration N_c near cloud top (scale above the box) and mean drop radius, $\bar{r}_c$, near cloud top (scale at the very bottom of the figure). The scales for both $\bar{r}_c$ and N_c are approximate as the cloud droplet concentration changes by a small amount depending on the concentration of giant aerosols; typically this effect is less than a few percent for N_c. The results for a total of 42 model runs with differing aerosol specifications are shown. The uncertainty resulting from the Monte Carlo scheme is examined below.

The Monte Carlo method is a fully stochastic method, and the result of the calculations depends on the initial seed number for the random number generator. A sequence of 20 runs was done to test the sensitivity to the seed number. The small aerosols were specified as $N_a = 200 \times 10^6\ S^{1.2}$ and the giant aerosols were specified for a wind speed of 8 m s^{-1}. The result was a standard deviation of the calculated rainfall rate at cloud base on descent of 0.000 22 mm h^{-1} for a mean rainfall rate of 0.002 68 mm h^{-1}; that is, the standard

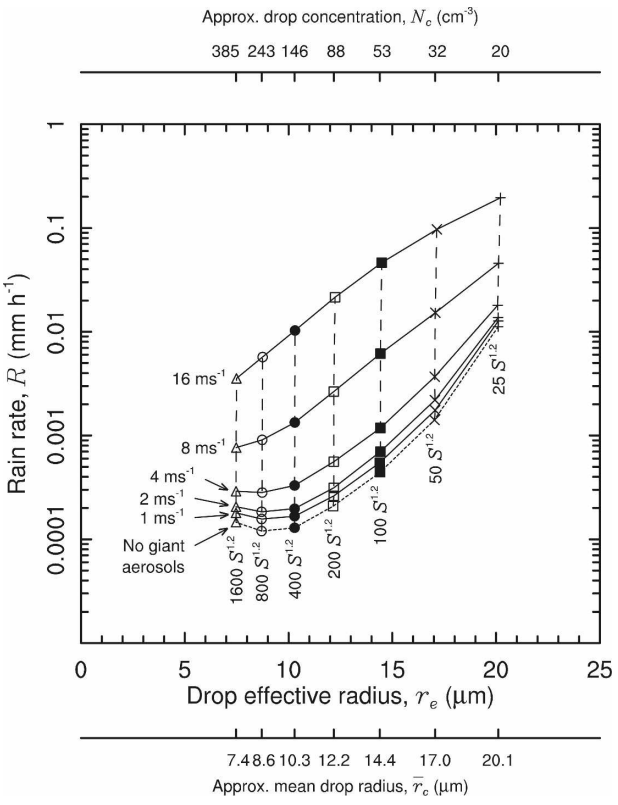

FIG. 6. Stratocumulus rain rate R at cloud base on descent as a function of cloud droplet effective radius r_e near cloud top (650 m). Each solid curve corresponds to a fixed wind-speed-dependent size distribution of giant and ultragiant sea-salt particles. Each long-dashed curve corresponds to a fixed aerosol size distribution calculated from CCN supersaturation spectrum (small aerosol particles); the individual labels correspond to a = 25, 50, 100, 200, 400, 800, and 1600 cm^{-3}, respectively, in the supersaturation spectrum, $N = aS^b$. The approximate mean radius $\overline{r_c}$ and cloud droplet concentrations N_c at cloud top are also shown.

deviation was 8% of the mean value. This is a small fraction of the total variability shown in Fig. 6 and it indicates that the numerical scheme yields robust results.

a. Giant versus small aerosol particles

The precipitation rate for a set of calculations without any giant aerosol particles (dotted line, bottom curve of Fig. 6) shows the smallest precipitation rates over the full range of size distributions of small aerosol particles.

Each of the solid curves in Fig. 6 corresponds to one size distribution of giant aerosol particles and a range of size distributions for the small aerosol particles. Following these solid curves from left to right shows an increase in rainfall rate of about two orders of magnitude as the effective radius is increased from ~7 to 20 μm.

Each of the dashed curves (near-vertical in Fig. 6) corresponds to one size distribution of small aerosol particles and a range of size distributions for the giant aerosol particles. Moving upward along each of the dashed curves shows an increase in rainfall rate of about two orders of magnitude as the wind speed is increased (more giant sea-salt aerosol particles). This is particularly the case for the common intermediate concentrations of small aerosol particles; the impact of giant aerosols is reduced for very polluted air and very clean air (far left and right sides, respectively, of Fig. 6).

The total variability of the calculated rainfall rate is thus three orders of magnitude; two orders of magnitude variability can be explained by smaller aerosol particles ($r_d < 0.5$ μm) and two orders of magnitude can be explained by variability in giant aerosol particles ($r_d > 0.5$ μm). This makes the variability due to giant aerosols and the variability due to smaller aerosols of equal importance for the rainfall rate in this marine stratocumulus cloud. This is an unexpected but highly significant result, and it points to the need for accurate representation of giant sea-salt aerosols as part of warm rain formation in numerical models.

Figure 6 also shows that, for wind speeds in excess of 4–5 m s^{-1}, more than half the rainfall rate is caused by drops formed on giant aerosols. This can be seen by comparing the rainfall rates for the 4 m s^{-1} curve to that of the "no giant aerosol" curve. Thus, for wind speeds in excess of 4–5 m s^{-1}, the majority of the precipitation flux is carried by drops formed on giant sea-salt aerosols. Using the data shown in Fig. 8 it can be calculated that at 8 m s^{-1} the drops formed on giant aerosols carry 75%–91% of the total rain rate (dependent on droplet effective radius); at 16 m s^{-1}, the drops formed on giant aerosol particles carry 94%–99% of the total rain rate.

The results in Fig. 6 demonstrate a stronger dependency on the giant aerosol size distribution than was found by Feingold et al. (1999). The reason for this may be that the present calculations use a numerical scheme without artificial broadening, whereas the scheme developed by Tzivion et al. (1987) and used by Feingold et al. (1999) still has some numerical broadening despite its improvements over earlier moment-conserving schemes. It may also be a result of Feingold et al. using only a single size of giant aerosol particles, whereas the present study incorporates a full spectrum.

The effective drop radius at cloud top has been used to infer the state of warm rain development (Rosenfeld and Lensky 1998). Each of the dashed curves in Fig. 6 is nearly vertical, indicating that a wide range of rainfall rates is possible for nearly constant r_e, coincident with a highly varying amount of giant aerosol particles. The

conclusion is that there may be cases where the cloud-top effective radius is a poor indication of the state and magnitude of precipitation development in marine stratocumulus clouds. Although the rainfall rates in the present study are small, it should be noted that a given precipitation rate may result from values of r_e covering the entire range from 7 to 20 μm; that is, there is no critical drop radius above which precipitation forms. This is in contrast to the conclusions of Gerber (1996) and Rosenfeld and Lensky (1998); we note that these observational studies likely covered a much smaller parameter space in terms of supersaturation spectra and wind speeds than that used in the present study.

The adiabatic model predicts a full range of droplet spectral dispersions ($\sigma/\bar{r}_c$) of only 0.03–0.08 at cloud top, with the highest values occurring for very polluted (many small aerosol particles) and very windy (many giant aerosols) conditions. The increase in dispersion due to addition of giant aerosol particles is only 0.01–0.02 of the above values. Thus, the rainfall rate may increase by two orders of magnitude due to giant aerosols (see Fig. 6), but this is associated with a very small increase in the droplet dispersion at cloud top.

b. Enhanced droplet growth: Turbulence

Turbulent motion has been proposed as a mechanism for enhancing droplet coalescence (e.g., de Almeida 1979; Pinsky and Khain 1995; Franklin et al. 2005; Wang et al. 2006). Turbulent motions may also locally increase the droplet concentration, leading to enhanced coalescence rates (Shaw et al. 1998). The present model does not include any turbulence fields since coalescence is only calculated for gravitational forces. Direct numerical simulation (Franklin et al. 2005) has previously been used to estimate the increases in collision kernel for a turbulent cloud compared to that of a nonturbulent cloud using two drops of 10 and 20 μm radius to demonstrate the effect. Their calculations include both clustering and changes to the differential radial velocity due to turbulence. Franklin et al. found that the increase in collision kernel for a turbulent energy dissipation rate, $\epsilon = 95$ cm^2 s^{-3}, was 1.06 (i.e., quite small). The dissipation rate in stratocumulus is typically an order of magnitude smaller (Lothon et al. 2005), and it can thus expected that the effect of turbulence on coalescence in these clouds is very small.

Given the remaining uncertainty of the effect of turbulence on droplet coalescence, two sets of calculations were done for which all collision kernels were uniformly increased by factors of 1.1, 1.2, 1.5, and 2.0. The calculations were conducted for small aerosol particles specified as $N_a = 200 \times 10^6\ S^{1.2}$ m^{-3} and with two

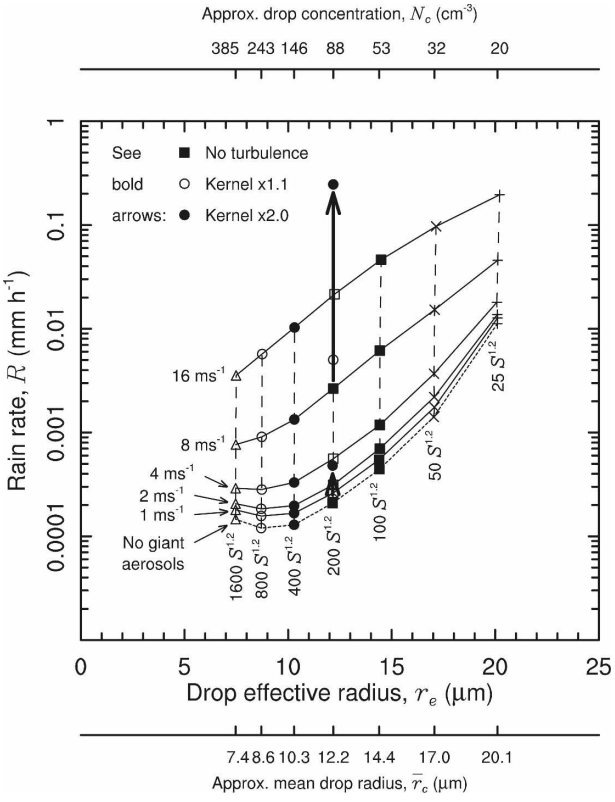

FIG. 7. As in Fig. 6 but with added results demonstrating the increase in rain rate R resulting from increases in collection kernel as a surrogate for turbulence. The two vertical arrows show the increase in collection kernel by factors of 1.1 and 2.0 over that of the standard kernel. The lower arrow represents a case with no giant aerosols, and the upper arrow a case with a giant aerosol distribution for an 8 m s^{-1} wind speed.

specifications for giant aerosol particles: no giant aerosol particles and giant aerosol particles corresponding to a marine wind speed of 8 m s^{-1}.

For the case of no giant aerosol particles (see Fig. 7), the result was that the rainfall rate at cloud base increased by factors of 1.1, 1.2, 1.5, and 2.3 respectively for the kernel enhancement factors mentioned previously, implying that turbulent enhancement to coalescence among drops formed on small aerosol particles is a very small effect in marine stratocumulus. Figure 4 shows that most small coalescence nuclei only capture one other drop; thus, higher collision efficiencies for drops formed on small aerosol particles primarily lead to more drops undergoing just one coalescence event. For the case of only small aerosols and turbulence, the increase in rainfall rate is nearly linear with the kernel enhancement factors.

For the case of giant aerosols specified corresponding to an 8 m s^{-1} wind speed, the resulting increases in rainfall rates were 1.9, 2.8, 10, and 93, respectively.

Thus, turbulent enhancement of the rainfall rate appears far more nonlinear and effective once giant aerosols are present; see Fig. 7. Nevertheless, for the turbulence levels expected in marine stratocumulus, enhanced turbulent coalescence is likely a very small effect.

c. *Enhanced droplet growth: Mixing and wide spectra*

It is sometimes assumed that adiabatic models, such as the one applied in the present study, cannot be used to simulate real clouds. This is because the adiabatic model assumption results in narrow calculated drop spectra, whereas observed drop spectra are broader. However, it is well known that observed drop spectra using common laser spectrometers [PMS Forward Scattering Spectrometer Probes (FSSPs)] are affected by significant instrumental broadening (e.g., Brenguier et al. 1998). Measurements from DYCOMS-II stratocumulus cloud tops using a normal FSSP show typical droplet spectral dispersions, $\sigma_r/\bar{r}_c$, of 0.2. In contrast, the adiabatic model predicts droplet spectral dispersions of only 0.03–0.08 at cloud top.

In the present study we do not consider entrainment that may lead to a widening of the droplet spectrum (e.g., Baker and Latham 1979; Telford and Chai 1980; Lasher-Trapp et al. 2005). The applicability of the adiabatic assumption was examined using the present model to create wider spectra through mixing cloudy parcels with different drop spectra (as opposed to entraining dry air from outside the cloud). In the absence of entrainment, the creation of wide droplet spectra is simulated to occur as a result of (i) mixing between cloudy parcels that experienced different updraft speeds at cloud base and (ii) mixing between cloudy parcels with different aerosol spectra. We do this for two idealized conditions; however, it should be noted that extreme scenarios are needed to create drop spectra with a similar width to that observed with standard FSSPs. In each case the results are compared to those of parcels with the same droplet effective radius.

1) MIXING PARCELS WITH DIFFERENT CLOUD-BASE UPDRAFT SPEEDS

If parcels with different updraft speeds at cloud base are mixed together at higher altitude in the cloud, then the mixed parcel may attain a wider drop spectrum. In Fig. 8 the solid curve shows the normal updraft profile from near surface (50 m) to near cloud top (650 m). To examine the effect of varying updrafts at cloud base, drop growth was calculated for two parcels with small

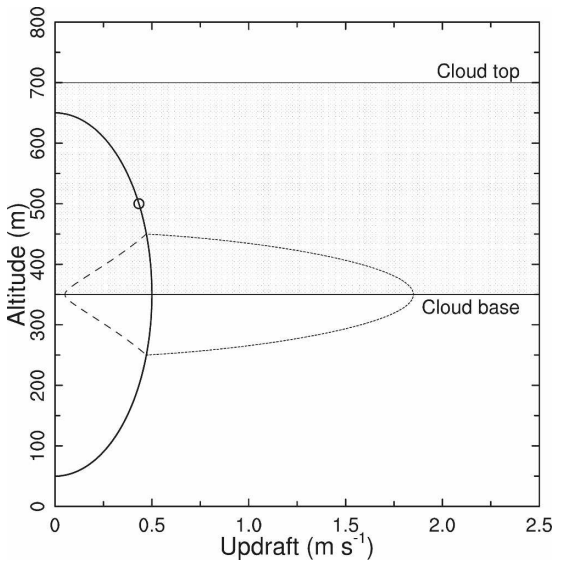

FIG. 8. Normal (solid curve) and perturbed (dashed and dotted curves) updraft profiles within 100 m of cloud base. These are used to create a mixed parcel with a wide drop spectrum at cloud top. The circle shows the altitude where the parcels are mixed 150 m above cloud base. For further details, see text.

aerosol particles specified by $N_a = 200 \times 10^6\, S^{1.2}$ m^{-3} and no giant aerosol particles. Their updraft profiles were perturbed with sine functions near cloud base z_b in the altitude range from $z_b - 100$ m to $z_b + 100$ m; see Fig. 8. One 8.5-L parcel was perturbed to have a cloud base velocity on ascent of 0.05 m s^{-1} at cloud base (dashed curve in Fig. 8), and a 1.5-L parcel was perturbed to have a cloud base updraft of 1.85 m s^{-1} (dotted curve in Fig. 8); this represents extreme deviations from the usual 0.5 m s^{-1} at cloud base but is necessary so as to create a wide drop spectrum at cloud top. The two parcels were mixed together at 150 m above cloud base and the remainder of the calculation follows the standard updraft profile to the cloud top and down again to the cloud base. The cloud parcel created by mixing as described above has a dispersion of 0.20 at cloud top, but the mixed parcel has a lower droplet concentration than the standard case with 0.5 m s^{-1} at cloud base; accordingly, the mixed parcel has a higher effective radius (15.1 μm) at cloud top than that of the standard case.

Once this mixed parcel has cycled back to cloud base, the resulting rainfall rate is only about a factor of 4 higher than that of the standard adiabatic parcel model for a parcel with the same cloud top effective radius; see Fig. 9. This extreme cloud base perturbation thus yields a small increase in rainfall rate compared to that with results from having giant aerosols corresponding to moderate marine wind speeds. In spite of the dramatic

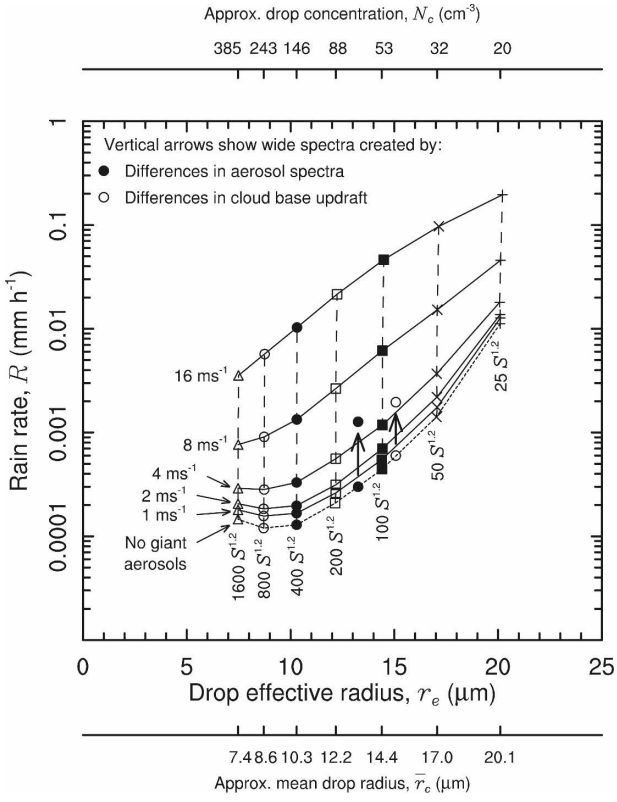

FIG. 9. As in Fig. 6 but with added results demonstrating the increase in rain rate R resulting (i) from mixing parcels with identical aerosol spectrum but with different updraft speeds at cloud base and (ii) from mixing cloudy parcels with different aerosol spectra but with identical updraft speed at cloud base. See text for further details.

widening of the droplet spectrum, the important conclusion is that, in the absence of giant aerosols, droplet spectral broadening for drops grown on small aerosol particles apparently does not lead to more than a modest precipitation rate increase over that calculated using a simple adiabatic model.

2) MIXING PARCELS WITH DIFFERENT AEROSOL SIZE DISTRIBUTIONS

Drop growth was calculated for eight parcels, each with its own specification of small aerosol particles (range $N_a = 50 \times 10^6\, S^{1.2}$ m^{-3} to $N_a = 6400 \times 10^6\, S^{1.2}$ m^{-3}) and without any giant aerosol particles. Cloud droplet growth was calculated for each of the eight parcels up to a level of 150 m above cloud base using the standard vertical velocity profile. Here the eight parcels were mixed together, and the resulting parcel was moved farther along the circular motion to near cloud top and then down again to cloud base. Using this extreme method to force drop spectrum broadening, a mixed parcel was created with a seven times broader drop spectrum at cloud top than that predicted with the simple adiabatic model (dispersions of 0.21 versus 0.03, respectively) and even wider drop spectra at lower altitudes (wider than observed at low levels in the DYCOMS-II clouds). In spite of this drastic widening in comparison to both the normal calculated adiabatic spectra and to the observed spectra, the mixed parcel shows only a factor of 4 increase in precipitation rate on descent at cloud base; see Fig. 9. In the absence of giant aerosols, we once again conclude that droplet spectral broadening for drops grown on small aerosol particles does not lead to more than a modest precipitation rate increase over that calculated using a simple adiabatic model.

d. Anthropogenic changes to rainfall rate

Changes to the aerosol populations will lead to precipitation rate changes for the modeled stratocumulus cloud. The evaluation of such changes has to be done under the simplifying assumption that no other conditions change.

Anthropogenic changes to aerosol populations may stem from both small and giant aerosol particles. If anthropogenic emissions only add small aerosol particles, with the same aerosol spectral shape and composition but higher concentrations, then the rainfall rate will be reduced by following the appropriate solid lines on Fig. 6 from the right toward the left. The average reduction in rainfall rate for a doubling of the small aerosol concentration is 42% (with a standard deviation of 29%). Expressed for a doubling of cloud droplet concentration, the average reduction in rainfall rate is 65% (with a standard deviation of 46%). This calculation is only appropriate for the cloudy parcel development of precipitation through the cloud and down to cloud base, and it does not apply to the rainfall that may or may not reach the ground. Nevertheless, the quantification points to the sensitivity of warm rain formation in marine stratocumulus to changes caused by anthropogenic increases of aerosol particles, assuming that all other conditions remain unchanged.

If the anthropogenic emission of aerosol particles consists of both small and giant aerosol particles, then it may be possible to increase the precipitation rate by, for example, moving from the lower right to the upper left of Fig. 6. However, to merely keep the precipitation rate constant for a case of doubling the concentration of small aerosol particles requires substantial additions of giant aerosol particles, especially if these giant aerosol particles were not of the same hygroscopic character as

sea salt. The exact calculations go beyond the scope of the present study.

e. Implications for climate prediction

Advanced climate mesoscale and large-scale models usually employ bulk microphysics; that is, they carry prognostic equations for mixing ratio of cloud water and other water categories. Based on the cloud water, they derive a rate of initial rain formation. This so-called autoconversion rate accounts for the change in rainwater mixing ratio due to small cloud droplets growing larger than the threshold size (e.g., 50-μm radius) assumed to separate cloud droplets from rain drops.

The autoconversion rate is calculated in several different ways in bulk microphysics models. Simple parameterization (Kessler 1969) invokes an autoconversion rate A, which depends on the liquid water mixing ratio q_l; that is, $A = f(q_l)$: Once q_l exceeds a threshold value, warm rain forms. More complex schemes [Manton and Cotton (1977); see Liu and Daum (2004) for an overview] predict warm rain formation based on two parameters, q_l and the cloud droplet mean radius $\bar{r}_c$; that is, $A = f(q_l, \bar{r}_c)$ where the cloud droplet radius must exceed a threshold size (e.g., 10 μm) for warm rain to form. It is clear that neither of these schemes can capture much of the variability displayed in Fig. 6.

Other autoconversion schemes also take into consideration spectral dispersion as well as liquid water (Berry and Reinhart 1973; Beheng 1994; Seifert and Beheng 2001; Liu and Daum 2004). They do, however, make assumptions about the width of the cloud droplet size distribution, and this assumption is critical to the result of their calculations. In the present study we do not make assumptions about the width of the drop size distribution; instead, we start with an aerosol size distribution and calculate the actual drop size distribution.

The present calculations, demonstrating a strong dependence of giant aerosol particles, suggest that the autoconversion rate should depend on three parameters: q_l, $\bar{r}_c$, and giant sea-salt aerosol spectrum χ_s; that is, the functional relationship is $A = f(q_l, \bar{r}_c, \chi_s)$. For the modeled marine stratocumulus it should be noted that the rainfall formation, and thus autoconversion rate, is equally dependent on χ_s and $\bar{r}_c$. The observations and modeling studied required for the development of such an autoconversion rate goes beyond the present paper, but the importance of giant aerosol particles for warm rain formation in climate and other large-scale models should not be ignored. It should also be noted that these models must accurately predict the concentrations and sizes of giant aerosols, or the calculation of rain rate will be in error.

6. Summary and discussion

A cloud model has been developed with simple dynamics (prescribed air motion, adiabatic transport, particles remaining in the air parcel) and highly complex microphysics (condensation, stochastic Monte Carlo coalescence, and tracing of aerosols through coalescence events). The model is applied to a typical marine stratocumulus of moderate thickness; for thicker clouds it can be expected that the calculated rain rates will be higher. All runs produce the same maximum liquid water of 0.59 g kg^{-1}, which is realistic in comparison to observations of marine stratus (Stevens et al. 2003a). The kinematic nature of the model also ensures that all simulated parcels spend the same amount of time in cloud ($\sim$31 min).

An extensive set of calculations is performed in which the size spectra of small sulfate aerosols are varied to simulate natural and anthropogenic variations in the aerosol particles that form the majority of cloud droplets. The combined size spectrum of giant and ultragiant aerosol particles is varied independently to simulate the natural variation in large sea-salt particles caused by breaking ocean waves. The parameter space includes very clean marine air to moderately polluted air; extremely polluted air (e.g., heavily biomass burn-effected air) is not included. The parameter space for giant sea-salt aerosol included wind speeds from calm to 16 m s^{-1}. For our goal of focusing on the rain rate of a cloud parcel when descended to cloud base, the main conclusions are as follows:

- The natural variability in wind speed causes large variations in the sizes and concentrations of giant and ultragiant aerosol particles, and this leads to a variation in rainfall rate that is of equal importance to the variation in rainfall rate caused by the natural and anthropogenic variations in smaller sulfate particles.
- For wind speed in excess of 4–5 m s^{-1}, drops initially formed on giant and ultragiant aerosol particles dominate the rainfall rate at cloud base. Many other coalescence drops result from coalescence of droplets initially formed on smaller sulfate particles, but these coalescence drops remain small in comparison to those initially formed on larger sea-salt particles. Thus, for more than modest wind speeds, the main droplet peak is for all intent and purposes merely "food" for the growth of the drops formed on giant and ultragiant aerosol particles.
- Addition of giant aerosols may cause a two order of magnitude increase in rainfall rate, but this is associated with a very small increase in the droplet spectral dispersion.
- For the case of only small aerosols, simple calcula-

tions of the effects of enhanced droplet growth caused by mixing-generated broad condensational spectra point to this effect as being relatively unimportant for the development of precipitation in warm marine stratocumulus.

- Increasing the collection kernel to simulate turbulent enhancement to gravitational kernels leads to either a negligible change in precipitation rate (when no giant aerosols are present) or a small change in precipitation rate (when giant aerosols are present). Turbulent enhancement to gravitational coalescence in marine stratocumulus is thus likely to be an unimportant effect owing to the low turbulence levels in these clouds.
- Doubling the concentrations of small aerosol particles, which can readily be caused by increased anthropogenic emissions, results in an average decrease of the precipitation rate at cloud base by 42%; this is a strong sensitivity to anthropogenic emissions and it may affect the cloud lifetime.
- To judge the state of precipitation development from the droplet effective radius (Rosenfeld and Lensky 1998) is not substantiated for the calculations presented here. This is because the small droplets (formed on small aerosol particles) dominate the effective radius calculation, whereas the few large drops (formed on giant aerosol particles) do not contribute significantly to the droplet effective radius. The variability in precipitation rate caused by variability in giant sea-salt particles is thus "masked" by the smaller cloud droplets when calculating the droplet effective radius.
- There is no mean or effective drop radius above which rain forms efficiently; rather, a continuum exists.
- Most current climate models do not include both important aerosol effects responsible for the formation of warm rain, that is, the size distribution of small and of giant aerosol particles. This casts doubt on the calculation of warm rain in such models and on the predicted magnitude of the cloud lifetime effect.

The present calculations use a particular set of aerosol size distributions, notably the Woodcock (1953) sea salt measurements. Other measurements have been made, yielding a range of size distributions (see Lewis and Schwartz 2005). Thus, usage of other aerosol size distributions (both small and large) may shift the calculated rainfall rates but is unlikely to change the conclusions regarding the importance of the giant sea salt aerosols on marine stratocumulus warm rain formation.

The above conclusions are also based on the results from a single stratocumulus case with an assumed updraft profile. Real cloud conditions vary in many ways (e.g., cloud depth, updraft, thermodynamic properties, time spent in cloud, mixing, etc.). Nevertheless, we believe that the conclusions are robust, and that other cloud conditions may merely increase or decrease the precipitation rate while not challenging the conclusion that, for a given cloud, both the small and the giant aerosol particles are of equal importance for the warm rain formation. The essence of the present study cloud can expressed as follows:

> The concentration of activated drops formed on small aerosol particles (CCN) determines to what extent a single giant sea-salt aerosol may be allowed to grow.
>
> The concentration and sizes of giant sea-salt particles determine—once the wind speed exceeds 4–5 m s^{-1}—the resulting rainfall rate.

The present study strongly suggests a shift toward the development, implementation, and verification of sea-salt-based warm rain initiation schemes into large-scale models of climatically important marine stratocumulus—without that, our confidence in the prediction of warm rain formation and its implications for the future climate will remain small.

Acknowledgments. The model development was mostly done while both authors were working for CSIRO; this work was supported by the Australian Greenhouse Office. The model setup for stratocumulus and the present calculations were done at NCAR. NCAR is sponsored by the National Science Foundation. Thanks are due to Drs. W. A. Cooper, D. Johnson, and L. Rotstayn for providing insightful comments on the paper. Two anonymous reviewers provided excellent comments that significantly improved the paper.

REFERENCES

Albrecht, B. A., 1989: Aerosols, cloud microphysics, and fractional cloudiness. *Science,* **245,** 1227–1230.

Ayers, G. P., and J. L. Gras, 1991: Seasonal relationship between cloud condensation nuclei and aerosol methane sulfonate in marine air. *Nature,* **353,** 834–835.

Baker, M. B., and J. Latham, 1979: The evolution of droplet spectra and the production of embryonic raindrops in small cumulus clouds. *J. Atmos. Sci.,* **36,** 1612–1615.

Barkstrom, B. R., 1978: Some effects of 8–12-μm radiant energy transfer on the mass and heat budgets of cloud droplets. *J. Atmos. Sci.,* **35,** 665–673.

Beard, K. V., 1976: Terminal velocity and shape of cloud and precipitation drops aloft. *J. Atmos. Sci.,* **33,** 851–864.

——, and H. T. Ochs III, 1983: Measured collection efficiencies for cloud drops. *J. Atmos. Sci.,* **40,** 146–153.

Beheng, K. D., 1994: A parameterization of warm cloud microphysical conversion processes. *Atmos. Res.,* **33,** 193–206.

Bennartz, R., 2007: Global assessment of marine boundary layer cloud droplet number concentration from satellite. *J. Geophys. Res.,* **112,** D02201, doi:10.1029/2006JD007547.

Berry, E. X., and R. L. Reinhart, 1973: Modeling of condensation and collection within clouds. Desert Research Institute Physical Sciences Publication 16, University of Nevada, 96 pp.

Bigg, E. K., J. L. Gras, and D. J. C. Mossop, 1995: Wind-produced submicron particles in the marine atmosphere. *Atmos. Res.,* **36,** 55–68.

Boers, R., and P. B. Krummel, 1998: Microphysical properties of boundary layer clouds over the Southern Ocean during ACE 1. *J. Geophys. Res.,* **103D** (13), 16 651–16 663.

——, J. B. Jensen, P. B. Krummel, and H. Gerber, 1996: Microphysical and radiative structure of wintertime stratocumulus clouds over the Southern Ocean. *Quart. J. Roy. Meteor. Soc.,* **122,** 1307–1339.

——, ——, and ——, 1998: Microphysical and short-wave radiative structure of stratocumulus clouds over the Southern OCEAN: Summer results and seasonal differences. *Quart. J. Roy. Meteor. Soc.,* **124,** 151–168.

Brenguier, J.-L., T. Bourrianne, A. D. Coelho, J. Isbert, R. Peytavi, D. Trevarin, and P. Weschler, 1998: Improvements of droplet size distribution measurements with the Fast-FSSP (Forward Scattering Spectrometer Probe). *J. Atmos. Oceanic Technol.,* **15,** 1077–1090.

Colón-Robles, M., R. M. Rauber, and J. B. Jensen, 2006: Influence of low-level wind speed on droplet spectra near cloud base in trade wind cumulus. *Geophys. Res. Lett.,* **33,** L20814, doi:10.1029/2006GL027487.

Davis, M. H., and J. D. Sartor, 1967: Theoretical collision efficiencies for small cloud droplets in Stokes flow. *Nature,* **215,** 1371–1372.

Davis, R. H., 1984: The rate of coagulation of a dilute polydisperse system of sedimenting spheres. *J. Fluid Mech.,* **145,** 179–199.

De Almeida, F. C., 1979: The effects of small-scale turbulent motions on the growth of a cloud droplet spectrum. *J. Atmos. Sci.,* **36,** 1557–1563.

Feingold, G., W. R. Cotton, S. M. Kreidenweis, and J. T. Davis, 1999: The impact of giant cloud condensation nuclei on drizzle formation in stratocumulus: Implications for cloud radiative properties. *J. Atmos. Sci.,* **56,** 4100–4117.

Franklin, C. N., P. A. Vaillancourt, M. K. Yau, and P. Bartello, 2005: Collision rates of cloud droplets in turbulent flow. *J. Atmos. Sci.,* **62,** 2451–2466.

Fukuta, N., and L. A. Walter, 1970: Kinetics of hydrometeor growth from a vapor-spherical model. *J. Atmos. Sci.,* **27,** 1160–1172.

Gerber, H., 1996: Microphysics of marine stratocumulus with two drizzle modes. *J. Atmos. Sci.,* **53,** 1649–1662.

Gillespie, D. T., 1975: An exact model for numerically simulating the stochastic coalescence process in a cloud. *J. Atmos. Sci.,* **32,** 1977–1989.

Gras, J. L., 1995: CN, CCN, and particle size in Southern Ocean air at Cape Grim. *Atmos. Res.,* **35,** 233–251.

Hansen, J. E., and L. E. Travis, 1974: Light scattering in planetary atmospheres. *Space Sci. Rev.,* **16,** 527–610.

Hegg, D. A., and P. V. Hobbs, 1992: Cloud condensation nuclei in the marine atmosphere: A review. *Nucleation and Atmospheric Aerosols,* E. N. Fukuta and E. Wagner, Eds., A. Deepak, 181–192.

Hocking, L. M., 1959: The collision efficiency of small drops. *Quart. J. Roy. Meteor. Soc.,* **85,** 44–50.

——, and P. R. Jonas, 1970: The collision efficiency of small drops. *Quart. J. Roy. Meteor. Soc.,* **96,** 722–729.

Howell, W. E., 1949: The growth of cloud drops in uniformly cooled air. *J. Meteor.,* **6,** 134–149.

Hudson, J. G., and Y. H. Xie, 1999: Vertical distribution of cloud condensation nuclei spectra over the summertime northeast Pacific and Atlantic Oceans. *J. Geophys. Res.,* **104D** (23), 30 219–30 229.

Jensen, J. B., and R. J. Charlson, 1984: On the efficiency of nucleation scavenging at cloud base. *Tellus,* **36B,** 367–375.

Johnson, D. B., 1982: The role of giant and ultragiant nuclei in warm rain initiation. *J. Atmos. Sci.,* **39,** 448–460.

Kessler, E., 1969: *On the Distribution and Continuity of Water Substance in Atmospheric Circulation. Meteor. Monogr.,* No. 32, Amer. Meteor. Soc., 84 pp.

Klett, J. D., and M. H. Davis, 1973: Theoretical collision efficiencies of cloud droplets at small Reynolds numbers. *J. Atmos. Sci.,* **30,** 107–117.

Lasher-Trapp, S. G., W. A. Cooper, and A. M. Blyth, 2005: Broadening of droplet size distributions from entrainment and mixing in a cumulus cloud. *Quart. J. Roy. Meteor. Soc.,* **131,** 195–220.

Lewis, E. R., and S. E. Schwartz, 2005: *Sea Salt Aerosol Production: Mechanisms, Methods, Measurements, and Models—A Critical Review. Geophys. Monogr.,* Vol. 152, Amer. Geophys. Union, 413 pp.

Liu, Y., and P. H. Daum, 2004: Parameterization of the autoconversion process. Part I: Analytical formulation of the Kessler-type parameterizations. *J. Atmos. Sci.,* **61,** 1539–1548.

Lothon, M., D. H. Lenschow, D. Leon, and G. Vali, 2005: Turbulence measurements in marine stratocumulus with airborne Doppler radar. *Quart. J. Roy. Meteor. Soc.,* **131,** 2063–2080.

Low, R. D. H., 1969: A generalized equation for the solution effect in droplet growth. *J. Atmos. Sci.,* **26,** 608–611.

Lu, M.-L., W. C. Connant, H. H. Johnson, V. Varutbangkul, R. C. Flagan, and J. H. Seinfeld, 2007: The marine stratus/stratocumulus experiment (MASE): Aerosol–cloud relationships in marine stratocumulus. *J. Geophys. Res.,* **112,** D10209, doi:10.1029/2006JD007985.

Manton, M. J., and W. R. Cotton, 1977: Formulation of approximate equations for modeling moist deep convection on the mesoscale. Colorado State University Atmospheric Science Paper 266, 63 pp.

O'Dowd, C. D., and M. H. Smith, 1993: Physicochemical properties of aerosols over the northeast Atlantic: Evidence for wind-speed-related submicron sea-salt aerosol production. *J. Geophys. Res.,* **98,** 1137–1149.

——, ——, I. E. Consterdine, and J. A. Lowe, 1997: Marine aerosol, sea-salt, and the marine sulphur cycle: A short review. *Atmos. Environ.,* **31,** 73–80.

Pawlowska, H., and J.-L. Brenguier, 2000: Microphysical properties of stratocumulus clouds during ACE-2. *Tellus,* **52B,** 868–887.

Peng, Y., U. Lohmann, R. Laitch, C. Banic, and M. Couture, 2002: The cloud albedo–cloud droplet effective radius relationship for clean and polluted clouds from RACE and FIRE.ACE. *J. Geophys. Res.,* **107,** 4106, doi:10.1029/2000JD000281.

Pinsky, M., and A. Khain, 1995: A model of homogeneous isotropic turbulent flow and its application for the simulation of cloud drop tracks. *Geophys. Astrophys. Fluid Dyn.,* **81,** 33–55.

Posselt, R., and U. Lohmann, 2007: Influence of giant CCN on warm rain processes in the ECHAM5 GCM. *Atmos. Chem. Phys. Discuss.,* **7,** 14 767–14 811.

Pruppacher, H. R., and J. D. Klett, 1978: *Microphysics of Clouds and Precipitation.* D. Reidel, 714 pp.

Robinson, R. A., and R. H. Stokes, 1959: *Electrolyte Solutions: The Measurement and Interpretation of Conductance, Chemical Potential, and Diffusion in Solutions of Simple Electrolytes.* 3d ed. Butterworths Scientific Publications, 571 pp.

Rogers, J. R., and R. H. Davis, 1990: The effect of van der Waals attractions on cloud droplet growth by coalescence. *J. Atmos. Sci.,* **47,** 1075–1080.

Rosenfeld, D., and I. M. Lensky, 1998: Satellite-based insight into precipitation formation processes in continental and maritime convective clouds. *Bull. Amer. Meteor. Soc.,* **79,** 2457–2476.

——, R. Lahav, A. Khain, and M. Pinsky, 2002: The role of sea spray in cleansing air pollution over ocean via cloud processes. *Science,* **297,** 1667–1670.

Rotstayn, L. D., and Y. Liu, 2005: A smaller global estimate of the second indirect aerosol effect. *Geophys. Res. Lett.,* **32,** L05708, doi:10.1029/2004GL021922.

Rudich, Y., O. Khersonsky, and D. Rosenfeld, 2002: Treating clouds with a grain of salt. *Geophys. Res. Lett.,* **29,** 2060, doi:10.1029/2002GL016055.

Schlamp, R. J., S. N. Grover, H. R. Pruppacher, and A. E. Hamielec, 1976: A numerical investigation of the effect of electric charges and vertical external electric fields on the collision efficiency of cloud drops. *J. Atmos. Sci.,* **33,** 1747–1755.

Seifert, A., and K. D. Beheng, 2001: A double-moment parameterization for simulating autoconversion, accretion, and self-collection. *Atmos. Res.,* **59,** 265–281.

Shaw, R. A., W. C. Reade, L. R. Collins, and J. Verlinde, 1998: Preferential concentration of cloud droplets by turbulence: Effects on the early evolution of cumulus cloud droplet spectra. *J. Atmos. Sci.,* **55,** 1965–1976.

Simpson, G. C., 1906: The velocity equivalents of the Beaufort scale. Met Office Publication 180. [Available in *Smithsonian Meteorological Tables,* 6th rev. ed. (2000), Smithsonian, 527 pp.]

Smith, M. H., I. E. Consterdine, and P. M. Park, 1989: Atmospheric loadings of marine aerosol during a Hebridean cyclone. *Quart. J. Roy. Meteor. Soc.,* **115,** 383–395.

Stevens, B., and Coauthors, 2003a: Dynamics and chemistry of marine stratocumulus—DYCOMS-II. *Bull. Amer. Meteor. Soc.,* **84,** 579–593.

——, and Coauthors, 2003b: Dynamics and chemistry of marine stratocumulus—DYCOMS-II: Flight summaries. *Bull. Amer. Meteor. Soc.,* **84** (Suppl.), S12–S25.

——, G. Vali, K. Comstock, R. Wood, M. van Zanten, P. H. Austin, C. S. Bretherton, and D. H. Lenschow, 2005: Pockets of open cells and drizzle in marine stratocumulus. *Bull. Amer. Meteor. Soc.,* **86,** 51–57.

Szumowski, M. J., R. M. Rauber, and H. T. Ochs III, 1999: The microphysical structure and evolution of Hawaiian rainbands. Part III: A test of the ultragiant nuclei hypothesis. *J. Atmos. Sci.,* **56,** 1980–2003.

Telford, J. W., and S. K. Chai, 1980: A new aspect of condensation theory. *Pure Appl. Geophys.,* **118,** 720–742.

Twomey, S., 1977: The influence of pollution on the shortwave albedo of clouds. *J. Atmos. Sci.,* **34,** 1149–1152.

Tzivion, S., G. Feingold, and Z. Levin, 1987: An efficient numerical solution to the stochastic collection equation. *J. Atmos. Sci.,* **44,** 3139–3149.

Van den Heever, S. C., G. G. Carrió, W. R. Cotton, P. J. DeMott, and A. J. Prenni, 2006: Impacts of nucleating aerosol on Florida storms. Part I: Mesoscale simulations. *J. Atmos. Sci.,* **63,** 1752–1775.

Wang, L.-P., Y. Xue, O. Ayala, and W. W. Grabowski, 2006: Effects of stochastic coalescence and air turbulence on the size distribution of cloud droplets. *Atmos. Res.,* **82,** 416–432.

Woodcock, A. H., 1950: Condensation nuclei and precipitation. *J. Meteor.,* **7,** 161–162.

——, 1953: Salt nuclei in marine air as a function of altitude and wind force. *J. Meteor.,* **10,** 362–371.

——, R. A. Duce, and J. L. Moyers, 1971: Salt particles and raindrops in Hawaii. *J. Atmos. Sci.,* **28,** 1252–1257.

Woods, J. D., and B. J. Mason, 1964: Experimental determination of collection efficiencies for small water droplets in air. *Quart. J. Roy. Meteor. Soc.,* **90,** 373–381.

Yum, S. S., and J. G. Hudson, 2004: Wintertime/summertime contrasts of cloud condensation nuclei and cloud microphysics over the Southern Ocean. *J. Geophys. Res.,* **109,** D06204, doi:10.1029/2003JD003864.